Molecular Vision 2016; 22:933-943 <http://www.molvis.org/molvis/v22/933>
Received 31 October 2015 | Accepted 29 July 2016 | Published 31 July 2016

Quantitative proteomics analysis with iTRAQ in human lenses with nuclear cataracts of different axial lengths

Haiyan Zhou,[1,2] Hong Yan,[1,3] Weijia Yan,[4] Xinchuan Wang,[5] Yong Ma,[2] Jianping Wang[2]

[1]Department of Ophthalmology, Tangdu Hospital, Fourth Military Medical University, Xi'an, China,; [2]Department of Ophthalmology, Shaanxi Provincial People's Hospital, Xi'an, China,; [3]Chongqing Key Laboratory of Ophthalmology, Chongqing Eye Institute, the First Affiliated Hospital, Chongqing Medical University, Chongqing, China.; [4]Department of Clinical Medicine, Xi'an Medical University, Xi'an, China,; [5]Department of Neurosurgery, Tangdu Hospital, Fourth Military Medical University, Xi'an, China

Purpose: The goal of this study was to identify and quantify the differentially expressed proteins in human nuclear cataract with different axial lengths.

Methods: Thirty-six samples of human lens nuclei with hardness grade III or IV were obtained during cataract surgery with extracapsular cataract extraction (ECCE). Six healthy transparent human lens nuclei were obtained from fresh healthy cadaver eyes during corneal transplantation surgery. The lens nuclei were divided into seven groups (six lenses in each group) according to the optic axis: Group A (mean axial length 28.7±1.5 mm; average age 59.8±1.9 years), Group B (mean axial length 23.0±0.4 mm; average age 60.3±2.5 years), Group C (mean axial length 19.9±0.5 mm; average age 55.1±2.5 years), Group D (mean axial length 28.7±1.4 mm; average age 58.0±4.0 years), Group E (mean axial length 23.0±0.3 mm; average age 56.9±4.2 years), and Group F (mean axial length 20.7±0.6 mm; average age 57.6±5.3 years). The six healthy transparent human lenses were included in a younger group with standard optic axes, Group G (mean axial length 23.0±0.5 mm; average age 34.7±4.2 years).Water-soluble, water-insoluble, and water-insoluble–urea-soluble protein fractions were extracted from the samples. The three-part protein fractions from the individual lenses were combined to form the total proteins of each sample. The proteomic profiles of each group were analyzed using 8-plex isobaric tagging for relative and absolute protein quantification (iTRAQ) labeling combined with two-dimensional liquid chromatography tandem mass spectrometry (2D-LC-MS/MS). The data were analyzed with ProteinPilot software for peptide matching, protein identification, and quantification. Differentially expressed proteins were validated with western blotting.

Results: We employed biological and technical replicates and selected the intersection of the two sets of results, which included 40 proteins. From the 40 proteins identified, six were selected as differentially expressed proteins closely related to axial length. The six proteins were gap junction alpha-3 protein, beta-crystallin B2, T-complex protein 1 subunit beta, gamma-enolase, pyruvate kinase isozymes M1/M2, and sorbitol dehydrogenase. Levels of beta-crystallin B2 expression were decreased in nuclear cataracts with longer axial length. The results of the mass spectrometric analysis were consistent with the western blot validation.

Conclusion: The discovery of these differentially expressed proteins provides valuable clues for understanding the pathogenesis of axial-related nuclear cataract. The results indicate that beta-crystallin B2 (CRBB2) may be involved in axial-related nuclear cataract pathogenesis. Further studies are needed to investigate the correlation between CRBB2 and axial-related nuclear cataract.

Cataract is the main cause of blindness and visual impairment in developing countries [1]. The global burden of cataract has been estimated at 196 disability-adjusted life years per 10,000 persons [2]. As the global population ages, cataract-induced visual dysfunction and blindness will increase [3]. Although cataract surgery is the most common and successfully performed operation, apart from the possibility of developing post-operative complications, cataract surgery itself poses a major economic burden. Measures for preventing and delaying cataract formation remain an active field of research. As cataract tends to occur in relatively young people, the relationship between axial myopia and nuclear cataract has received widespread attention. Axial myopia is also a potentially blinding disease. The public health burden of pathological myopia may be uniquely high in Asian countries [4]. A longer axial length is one of the important risk factors predisposing to lenticular progressive myopia. Pathological axial elongation leads to a change in the eyeball structure and has greatly increased the incidence of many complications, such as glaucoma, nuclear cataract, and

Correspondence to: Hong Yan, Department of Ophthalmology, Tangdu Hospital, Fourth Military Medical University, Xi'an 710038, Chongqing Key Laboratory of Ophthalmology, Chongqing Eye Institute, the First Affiliated Hospital, Chongqing Medical University, Chongqing 400016, China; Phone: +86-29-84777445; FAX: +86-29-84777445; email: yhongb@fmmu.edu.cn

retinal detachment [5]. Nuclear sclerotic cataract is a cause of visual loss in young patients with axial myopia. Many population-based and clinic-based studies have shown a close association between axial myopia and the onset of nuclear cataract [6,7]. Patients with axial myopia are more likely to develop cataracts at an earlier age than those with shorter axial lengths [8,9]. Increase in axial length myopia of the eye has been associated with a lower mean age at the time of surgery and a higher grade of nuclear cataract [10]. In myopic eyes, it has been hypothesized that the longer vitreous cavity may inhibit the oxidative defense system [9-11]. Hyperbaric oxygen treatment increases the risk of nuclear cataract formation [12-14], which strongly supports the oxidative theory of nuclear cataract formation. Previous reports have shown that levels of O_2 in the vitreous cavity increase following pars plana vitrectomy [15]. The frequent occurrence of nuclear cataract after pars plana vitrectomy may also be caused by an increase in intraocular oxygen tension. In severe myopia, posterior vitreous detachment (PVD) develops increasingly with age and the degree of myopia. Vitreous liquefaction is seen as one of the major causes of PVD. There is increasing evidence that PVD may increase vitreous oxygen levels [16-18]. Therefore, myopia increases the extent of vitreous liquefaction, which is important in the pathogenesis of nuclear cataract.

Axial myopia is complicated by the frequent and early development of nuclear cataracts, but the mechanism is unknown. Previous studies have identified some changes in proteins, in view of the causal relationship of myopia and nuclear cataracts. Boscia et al. [19] found lower plasma thiol (PSH) content in cataractous and even in clear lenses removed from patients with myopia and diabetes. The decrease in PSH concentration occurred earlier in diabetic patients and in patients with myopic cataract than in patients with senile cataract. Higher oxidative consumption of glutathione (GSH) has also been found in myopic cataracts compared with senile cataracts [20]. The basic research on axial-related nuclear cataract, however, does not include any related reports.

The crystalline lens contains high levels of proteins, and any change in the structure or amount of specific crystallins can lead to a cataract [21-24]. Therefore, proteomic technology is a useful research tool for illuminating the normal physiological and pathological changes in lens proteins, and it has been frequently used in research on cataracts [25]. The traditional approach in proteomic analysis includes isoelectric focusing/sodium dodecyl sulfate–polyacrylamide gel electrophoresis (IEF/SDS–PAGE) with mass spectroscopy. Although two-dimensional electrophoresis is the most frequently used technology for protein separation, there are still several problems to be overcome. The shortcomings of IEF restrict its widespread application [26]. Isobaric tagging for relative and absolute protein quantification (iTRAQ) is a newly developed proteomics technique for studying quantitative changes in proteins in different biological samples. iTRAQ labeling combined with two-dimensional liquid chromatography tandem mass spectrometry (2D-LC-MS/MS) is a standard technique for high-throughput protein identification and relative quantification. We have analyzed differentially expressed proteins in nuclear cataractous lenses and transparent lenses from people of different ages using LC-MS/MS and iTRAQ labeling, and the results suggest the importance of some proteins in contributing to the formation of cataract with aging [27].

Based on our previous study on the formation of nuclear cataract with aging, using iTRAQ, the purpose of this investigation was to identify and quantify the differentially expressed proteins in nuclear cataract with different axial lengths. This study may lead to further understanding of the role of the target proteins involved in the pathogenesis of axial-related nuclear cataract. These data may therefore be helpful in studying the pathological mechanisms of human axial-related nuclear cataract.

METHODS

The study protocol conformed to the tenets of the Declaration of Helsinki (2008 version) and was approved by the Ethics Committee of Tangdu Hospital, the Fourth Military Medical University. It conformed to the standards in the ARVO (Association for Research in Vision and Ophthalmology) Statement on human subjects. Written informed consent was obtained from all study participants. Lens opacity was diagnosed before surgery by a surgeon (the corresponding author) and a trained ophthalmologist (the first author) using the lens opacity classification system (LOCS) II [28]. Thirty-six samples of human lens nuclei from patients with hard nuclear cataracts were obtained during cataract surgery at the Disabled Rehabilitation Center in Qinghai Province, China. Extracapsular cataract extraction was employed to remove the cortical region, followed by irrigation and aspiration to extract the nuclear region. Lens nuclei were rapidly frozen in liquid nitrogen (−196 °C) until use. Six healthy transparent human lens nuclei were obtained from fresh healthy cadaver eyes during corneal transplantation surgery. The core of each lens was separated as stated in our previous work [22].The samples were stored as described above. All experimental samples were obtained from patients with lenses of different axial lengths and divided into groups with longer axis length

Table 1. Information on the 7 groups enrolled in the iTRAQ label.

Group	Specimen	Average age (year)	Mean axial lengths (mm)	Lens nucleus condition (LOCS II)	Gender F: female; M: male	iTRAQ label
A	6	59.8 ±1.9	28.7±1.5	IVdegree	2M4F	114
B	6	60.3±2.5	23.0±0.4	IIIdegree	2M4F	115
C	6	55.1±2.5	19.9±0.5	IIIdegree	3M3F	116
D	6	58.0±4.0	28.7±1.4	IVdegree	4M2F	117
E	6	56.9±4.2	23.0±0.3	IIIdegree	3M3F	118
F	6	57.6±5.3	20.7±0.6	IIIdegree	2M4F	119
G	6	34.7±4.2	23.0±0.5	transparent lenses	6M	121

(A, D), standard axis length (B, E), and shorter axial length (C, F; Table 1):

Group A: mean axial length 28.7±1.5 mm; average age 59.8±1.9 years, grade IV on the LOCS II scale, n = 6;

Group B: mean axial length 23.0±0.4 mm; average age 60.3±2.5 years, grade III on the LOCS II scale, n = 6;

Group C: mean axial length 19.9±0.5 mm; average age 55.1±2.5 years, grade III on the LOCS II scale, n = 6;

Group D: mean axial length 28.7±1.4 mm; average age 58.0±4.0 years, grade IV on the LOCS II scale, n = 6;

Group E: mean axial length 23.0±0.3 mm; average age 56.9±4.2 years, grade III on the LOCS II scale, n = 6;

Group F: mean axial length 20.7±0.6 mm; average age 57.6±5.3 years, grade III on the LOCS II scale, n = 6.

Six healthy transparent human lenses were included in a group of younger age with healthy optic axes, Group G: mean axial length 23.0±0.5 mm; average age 34.7±4.2 years.

Eyes with ocular risk factors for the development of cataracts (e.g., diabetes, history of ocular surgery, retinal detachment, uveitis, retinitis pigmentosa, vitreous hemorrhage, and some diseases that require steroid therapy) were excluded.

Extraction of WS, WI, and WI-US protein fractions: The experimental design is illustrated in Figure 1. Each lens sample was placed in a grinding mortar precooled with liquid nitrogen and manually ground under liquid nitrogen until the nitrogen evaporated and the mix was a fine, dry powder. Before the powder began to thaw, more liquid nitrogen was added, and the samples were ground two more times. From each lens, freeze-dried powder was isolated using the procedure described by Harrington et al. [29-32].

All procedures were performed at 4 °C unless indicated otherwise. The freeze-dried powder from each lens was thawed on ice, suspended (2 ml/lens) in Buffer A (50 mM Tris–HCl, pH 7.3, containing 1 mM dithiothreitol [DTT], 1 mM iodoacetamide, and 1 mM phenyl methane sulfonyl fluoride [PMSF]), and homogenized. The lens homogenate was centrifuged at 10,000 ×*g* for 15 min. The supernatant was recovered, and the pellet was homogenized and centrifuged three times. The supernatants recovered after each centrifugation were pooled and designated as the water-soluble (WS) protein fraction. The pellet designated as the water-insoluble (WI) protein fraction was suspended (2 ml/lens) in Buffer B (50 mM Tris–HCl, pH 7.9, 6 M urea, and 5 mM DTT) and homogenized. Subsequently, the suspension was centrifuged at 10,000 ×*g* for 15 min. The supernatant was recovered, and the pellet was homogenized and centrifuged three times. The supernatants were pooled and designated as the water-insoluble–urea-soluble (WI-US) protein fraction. After urea solubilization of the proteins, the residual pellet was suspended in buffer C (50 mM Tris–HCl, pH 7.9) and designated the water-insoluble–urea- insoluble (WI-UI) protein fraction. The three protein fractions from the individual lenses were combined to form the total proteins of each sample. The total protein concentration of each sample was determined using the Bradford protein assay. To diminish the effect of sample biological variation on the results of the proteomics analysis, the total proteins from six lenses in each group were pooled; consequently, there were two biological replicates in the longer axis length group, the standard axis length group, and the shorter axis length group, respectively.

iTRAQ labeling: The proteins were precipitated using a Ready Prep 2-D Clean up Kit (Bio-Rad Laboratories, Inc., Hercules, CA) according to the instructions. After precipitation, the protein pellets were resuspended in dissolution buffer from the iTRAQ kit. Protein quantification of each sample was performed using the Bradford protein assay [33]. Trypsin digestion and iTRAQ labeling were performed according to

the kit protocol (Applied Biosystems, Foster, CA). Briefly, 100 µg protein from each group was digested overnight at 37 °C with trypsin (MS grade; Promega). Following this, iTRAQ labeling was performed using an iTRAQ Reagent 8-Plex kit (P/N 4381663, LOT N: A3056, Applied Biosystems) based on the manufacturer's protocol (Table 1). For the longer axis length, standard axis length, and shorter axis length groups, two biological replicates were included. The two longer axis length groups (A, D) were labeled with iTRAQ reagents 114 and 117, the two standard axis length groups (B, E) were labeled with iTRAQ reagents 115 and 118, and the two shorter axial length groups (C, F) were labeled with iTRAQ reagents 116 and 119, respectively. The transparent lens group (G) was labeled with iTRAQ reagent 121.

2D-LC conditions: Chromatographic separation of the pooled samples was performed on a 20AD high-performance liquid chromatography (HPLC) system (Shimadzu; Kyoto, Japan). Tryptically digested and labeled peptides were first fractionated using a strong cation exchange liquid chromatograph on a 2.1 mm × 150 mm, 3.5 µm, 300 Å column (Waters Corporation, Milford, MA). The sample was loaded onto the column and eluted stepwise by injecting salt plugs of ten molar concentrations (25, 50, 75, 100, 150, 200, 300, 400, 500, and 1,000 mM NH_4Ac). Ten fractions were collected from the strong cation exchange column. Each fraction was then loaded across a ZORBAX 300SB-C18 RP column (5 µm, 300 Å, 0.1 × 150 mm; Michrom BioResources, Auburn, CA) and analyzed on a QSTAR XL System (Applied Biosystems) coupled with a 20AD HPLC system (Shimadzu). The flow rate used for separation on the reversed-phase (RP) column was 0.4 ml/min. Buffer A consisted of 5% acetonitrile, 95% water, and 0.1% formic acid; Buffer B consisted of 95%

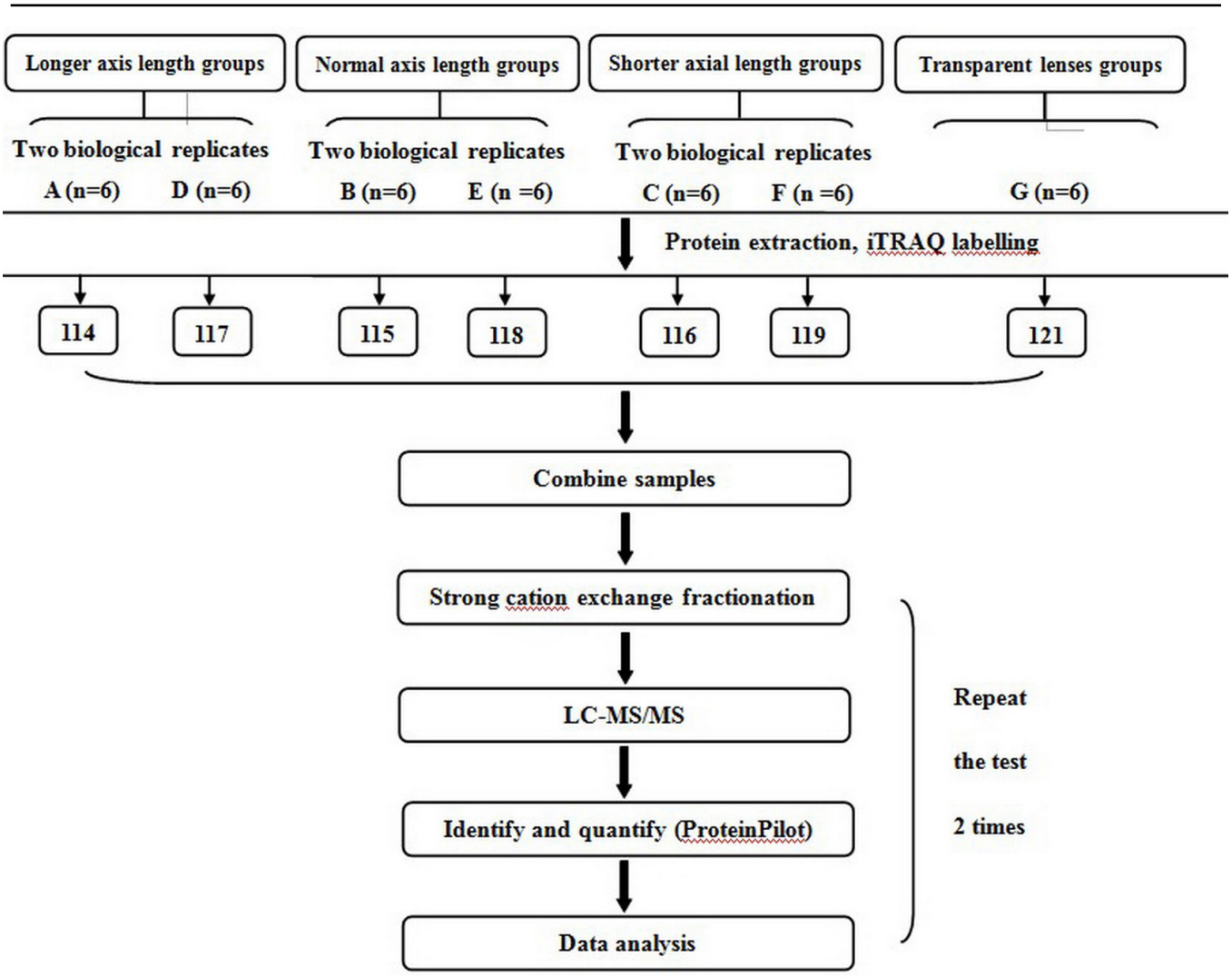

Figure 1. The experimental design workflow.

acetonitrile, 5% water, and 0.1% formic acid. Elution was performed using a gradient ranging from 5% to 45% of Buffer B over 90 min [34].

MS/MS conditions: The LC eluent was subjected to positive ion nanoflow electrospray analysis using a Qstar XL MS/MS system (Applied Biosystems) in the information-dependent acquisition mode (IDA). Time-of-flight (TOF)-MS survey scans were obtained with m/z ranges of 400–1,800 for MS with up to four precursors selected from m/z 100–2,000 for MS/MS. Product ion spectra were accumulated for 2 s in the mass range m/z 100–2,000 with a modified Enhance All mode. The Q2 transition settings favored low mass ions; thus, the reported iTRAQ ion intensities were enhanced for quantification. The iTRAQ-labeled peptides fragmented under collision-induced dissociation conditions to yield reporter ions at 113, 114, 115, 116, 117, 118, 119, and 121. The peak area ratios of the iTRAQ reporter ions reflected the relative abundances of the peptides. Protein expression ratios were computed based on the peak area ratios of the peptides accounting for the same protein. The LC-MS/MS step was repeated twice on the same set of samples.

Data analysis: Protein identification and iTRAQ quantification were performed with the ProteinPilot software version 4.5, revision number 1656 (Applied Biosystems). The data analysis parameters were set as follows: Sample type: iTRAQ (peptide labeled); Species: *Homo sapiens*; Digestion: Trypsin; Cys alkylation: methyl methanethiosulfonate; Instrument: QSTAR ESI; ID Focus: Biological modifications; Database: International Protein Index human database, version: 3.45; 143,958 entries); Search Effort: Thorough; Max missed cleavages: 2; FDR Analysis: Yes; User Modified Parameter Files: No; Bias Correction: Auto; and Background Correction: Yes. The identified proteins were grouped by the software to minimize redundancy. The identified proteins were grouped by the software to minimize redundancy. All peptides used to calculate the protein ratios were unique to the given protein or proteins within the group, and peptides that were common to other isoforms or proteins of the same family were ignored. The protein confidence threshold cutoff was 1.3 (unused ProtScore), with at least two peptides with 95% confidence. The false discovery rate for protein identification was calculated by searching against a reverse-concatenated database.

Western blot validation: The proteomic results obtained by iTRAQ coupled with 2D LC–MS/MS were validated using western blotting. Valuable Proteins was selected for this purpose. Western blotting was performed on new, different patient groups. Ten human lens nucleus samples with a hardness grade were obtained during cataract surgery. The samples were divided into two groups (five lenses in each group) according to axis length. The protein contents were determined with the bicinchoninic acid (BCA) assay (Bio-Rad, Hemel Hempstead, UK). A total of 20 µg of the protein samples were loaded onto 10% SDS-polyacrylamide gels and transferred to polyvinylidene difluoride membranes. The membrane was blocked with Tris-buffered saline (TBS; 10 mM Tris and 150 mM NaCl [pH 7.4]) containing 5% wt/vol skim milk 0.1% and Tween-20 (TBST) and then hybridized with a primary anti-CRBB2 antibody (Sigma, St. Louis, MO), followed by incubation with a horseradish peroxidase–conjugated secondary antibody (Jackson ImmunoResearch Laboratories, Inc ,West Grove, PA). β-Actin was used as a control for protein loading. Proteins were detected using a gel imaging and analysis system (ChemiDoc XRS, Bio-Rad).

RESULTS

Protein identification: Two technical replicates of iTRAQ analyses were carried out: 103 proteins were found in the first iTRAQ analysis, and 65 proteins were found in the second iTRAQ analysis. We chose the intersection of the two results, and thus, 40 proteins were detected.

Proteins that were observably and synchronously upregulated or downregulated (fold-change ≥1.2 or ≤0.8) in pairwise comparisons, 115:114 (B:A), 116:114 (C:A), 118:114 (E:A), 119:114 (F:A), 115:117 (B:D), 116:117 (C:D), 118:117 (E:D), and 119:117 (F:D), were regarded as potential differentially expressed proteins in the nuclear cataracts with longer axial length. A total of six proteins were selected as differentially expressed proteins closely related to axial length. Three proteins were found to be upregulated, and three were found to be downregulated in the shorter axis length group and the standard axis length group with nuclear cataracts, when compared with the groups with longer axis length and nuclear cataracts. The distribution of the differentially expressed proteins is shown in Table 2 and Table 3.

The ion assignments were as follows: iTRAQ 114 (A), 117 (D), nuclear cataract from the longer axis length groups; iTRAQ 115 (B), 118 (E), nuclear cataract from the standard axis length groups; iTRAQ 116 (C), 119 (F), nuclear cataract from the shorter axis length groups; and iTRAQ 121 (G), transparent lens from the group with younger age and standard axis length.

The MS/MS spectra of the representative peptides of beta-crystallin B2 (CRBB2), along with their reporter ions, obtained from the lens samples are shown in Figure 2. These ratios suggested that the relative protein abundance of CRBB2 was decreased in nuclear cataracts with longer axis length.

Molecular Vision 2016; 22:933-943 <http://www.molvis.org/molvis/v22/933>

Table 2. Differentially expressed proteins in the longer axial length groups (A=114) and the others groups with different axial length (B=115,C=116,E=118,F=119).

	Unused	Total	%Cov	Name	Peptides -0.95	Average fold change							
						115:114 B:A	p-value	116:114 C:A	p-value	118:114 E:A	p-value	119:114 F:A	p-value
1	57.25	57.55	100	Beta-crystallin B2	100	1.77	0.0013	1.27	0	2.01	0	1.92	0.0017
2	20.23	20.25	57.4	Gap junction alpha-3 protein	20	1.43	0.0001	1.67	0.0012	1.27	0.0039	1.42	0
3	15.53	15.66	44	T-complex protein 1 subunit beta	13	1.39	0.0001	1.55	0	1.37	0.0001	1.25	0.0001
4	12.12	12.22	31.1	Gamma-enolase	9	0.56	0.0001	0.36	0	0.35	0.0043	0.49	0.0324
5	10.82	10.88	47.8	Pyruvate kinase isozymes M1/M2	6	0.48	0.0041	0.67	0.0048	0.71	0.0022	0.55	0.0123
6	4.54	4.55	33.6	Sorbitol dehydrogenase	4	0.67	0.0022	0.25	0.0022	0.6	0.003	0.24	0

Shading: black, up-regulate; light gray, down-regulated. longer axial length (A=114, D=117), the normal axis length groups(B=115,E=118), the shorter axial length groups (C=116,F=119)

Table 3. Differentially expressed proteins in the longer axial length groups (D=117) and the others groups with different axial length (B=115,C=116,E=118,F=119).

	Unused	Total	%Cov	Name	Peptides	Average fold change							
						115:117		116:117		118:117		119:117	
					-0.95	B:D	p-value	C:D	p-value	E:D	p-value	F:D	p-value
1	57.25	57.55	100	Beta-crystallin B2	100	1.35	0	1.66	0	1.79	0.0011	1.32	0.0001
2	20.23	20.25	57.4	Gap junction alpha-3 protein	20	1.34	0	1.29	0.0034	1.47	0.0023	1.21	0.0022
3	15.53	15.66	44	T-complex protein 1 subunit beta	13	1.59	0.0033	1.27	0.0001	1.24	0.0001	1.41	0.0045
4	12.12	12.23	31.1	Gamma-enolase	9	0.76	0.018	0.35	0.0001	0.38	0.0044	0.59	0.0026
5	10.82	10.88	47.8	Pyruvate kinase isozymes M1/M2	6	0.34	0.0208	0.72	0.0034	0.69	0.0002	0.8	0.0033
6	4.54	4.55	33.6	Sorbitol dehydrogenase	4	0.75	0.0024	0.43	0.0026	0.79	0.0033	0.59	0.0047

Shading: black, up-regulate; light gray, down-regulated. longer axial length (A=114, D=117), the normal axis length groups(B=115,E=118), the shorter axial length groups (C=116,F=119)

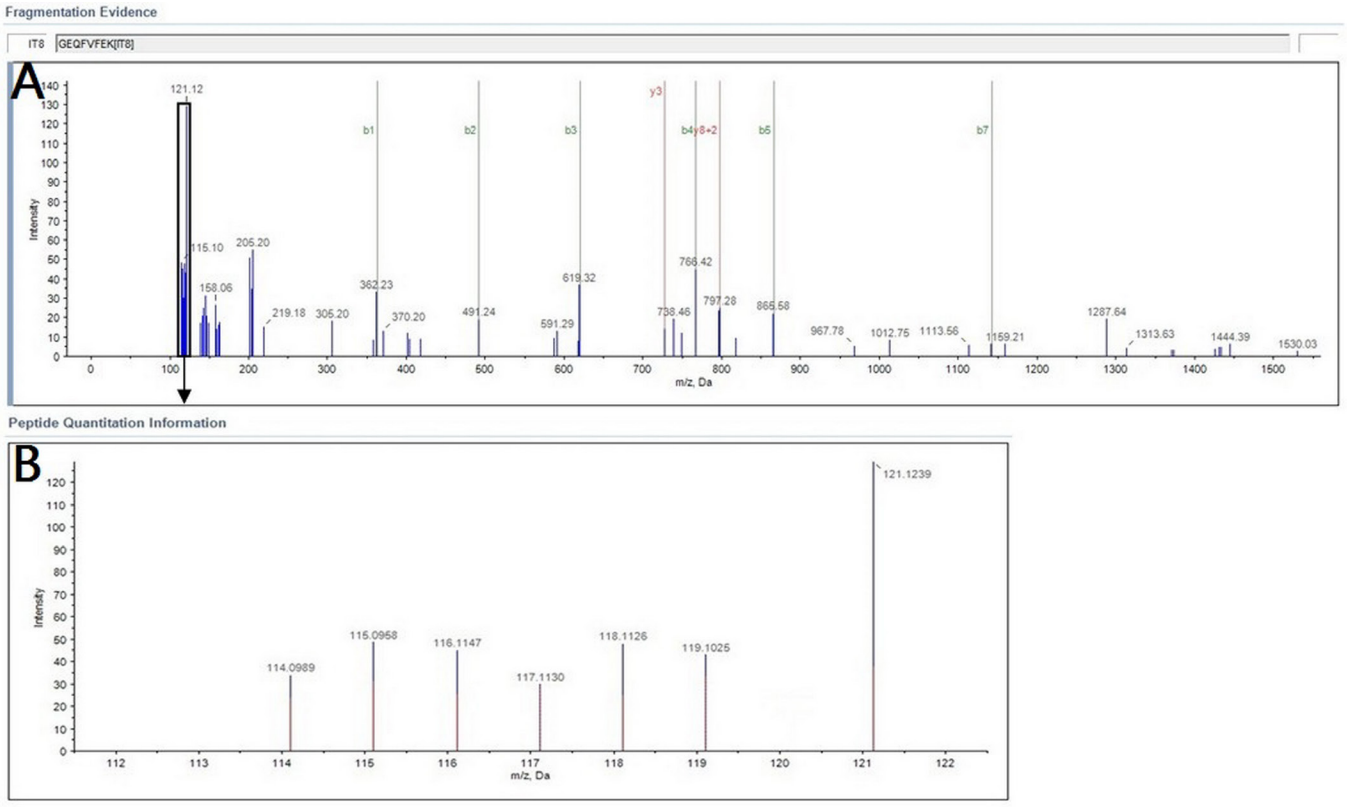

Figure 2. The MS/MS spectra of the representative peptides of CRBB2. **A**: A representative tandem mass spectrometry (MS/MS) spectrum for a peptide, GEQFVFEK, from CRBB2. **B**: The relative quantitative reporter ions, with the observed mass tags (114–121) indicating the relative abundance of this peptide in each group.

Validation of differently expressed proteins identified: CRBB2 was selected for this purpose. Ten human lens nucleus samples with a hardness grade were divided into two groups (five lenses in each group) according to axis length: Group X (mean axial length 23.1±0.8 mm; average age 57.3±3.2 years, grade II on the LOCS II scale) and Group Y (mean axial length 27.1±0.6 mm; average age 60.4±2.5 years, grade IV on the LOCS II scale; Table 4). The method described for extracting the protein fraction was used. The western blotting results were consistent with the MS analysis findings, validating the altered expression of CRBB2 in nuclear cataracts. The representative images and the relative band density of western blotting for CRBB2 are shown in Figure 3, and a densitometric analysis of the protein bands was performed using Quantity One software (Bio-Rad).

DISCUSSION

This study focused on the proteins present in nuclear cataracts with different axial lengths. We identified six differentially expressed proteins via iTRAQ labeling coupled with 2D-LC-MS/MS, and CRBB2 was selected to validate the proteomic results using western blotting. To our knowledge, such research has not been performed previously. We collected 36 samples of human cataract obtained during extracapsular cataract extraction (ECCE) procedures. After controlling for age, this experiment ruled out the possibility that the same proteins change in the formation of axial-related cataract.

Gap junction alpha-3 protein (connexin 46, GJA3) belongs to the connexin family and the alpha-type (group II)

Table 4. Information on the two groups enrolled in the western blot validation.

Group	Specimen	Average age (year)	mean axial lengths (mm)	lens nucleus condition (LOCS II)	Gender F: female; M: male
A	5	61.8 ±3.9	23.1±0.8	III degree	2M3F
B	5	60.4±2.5	27.1±0.6	IV degree	3M2F

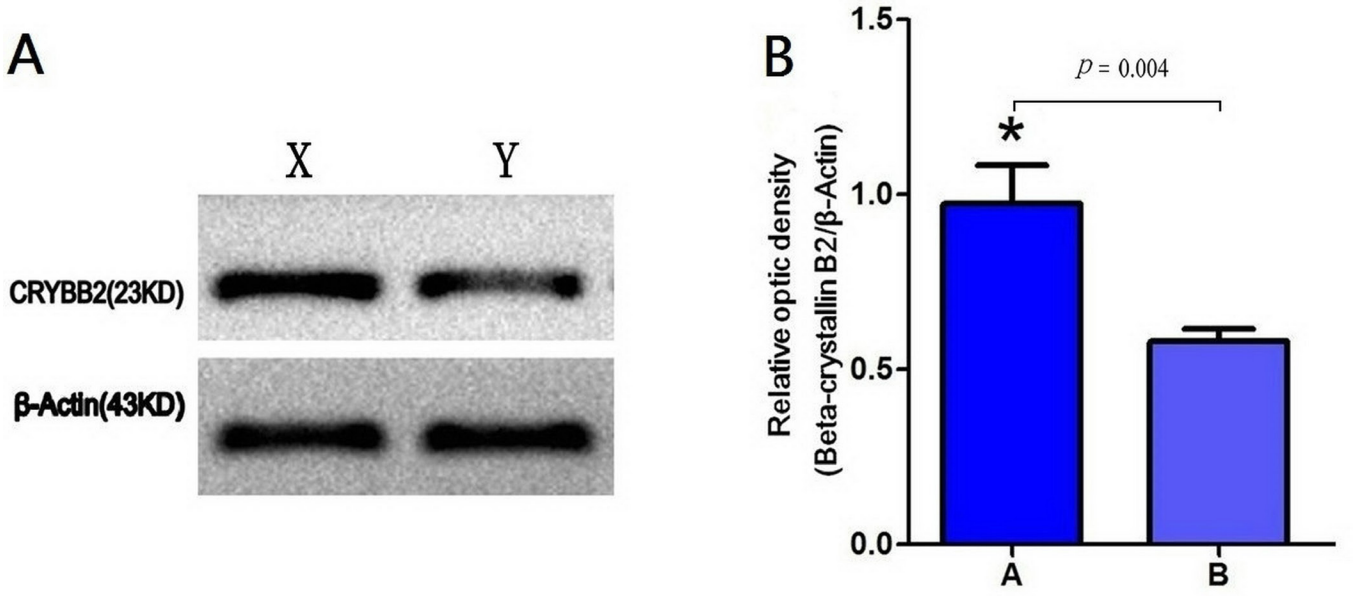

Figure 3. Western blot showing the levels of expression of CRBB2 in group A (standard axis length with nuclear cataract) compared with group B (longer axis length with nuclear cataract). β-Actin was used as a loading control. **A**: Representative images of the western blots. **B**: The expression of CRBB2 was decreased in the group with longer axis length nuclear cataract (A), *p< 0.05 versus group B (n = 5 per group).

subfamily. GJA3, the primary functional gap junction in the mature region of the lens, has been extensively studied in the mammalian lens [35-38]. Mutations in GJA3 have been linked with congenital cataract in humans [38] and mice [39-41]. We found that GJA3 was repeatedly upregulated in comparison with 115:114 (B:A), 116:114 (C:A), 118:114 (E:A), 119:114 (F:A), 115:117 (B:D), 116:117 (C:D), 118:117 (E:D), and 119:117 (F:D), indicating that the GJA3 content is lower in lenses with longer axial length than in other eyes. Further studies are needed to investigate the correlation between GJA3 and axial-related nuclear cataract by collecting new samples.

CRBB2, of the beta/gamma-crystallin family, is of particular interest because it is the major beta-crystallin in the mammalian lens. The *CRBB2* gene (HGNC ID: HGNC:2398; OMIM: 123620) is a late-expressed gene, which is expressed in rodents and humans only in the postnatal lens [42-44]. Our study showed that the levels of CRBB2 in the lenses with standard and shorter axial lengths were higher than those of the lenses with longer axial lengths. The high solubility of CRBB2 compared with the other β-crystallins suggests that it may play a unique role in maintaining lens transparency [45]. Human CRBB2 undergoes far less modification than other crystallins [46]. In aging lenses, the alpha-crystallins have become water-insoluble, and CRBB2 may play a dominant role in crystallin solubility in the lens. This resistance to modification leads to CRBB2 being the most soluble of the lens crystallins as the lens ages. Further studies are needed to investigate the correlation between CRBB2 and axial-related nuclear cataract.

The mechanism underlying the relationship between axial length and nuclear cataract is unclear and deserves further investigation. Intact vitreous gel is of critical importance to maintaining the low level of oxygen around the lens by preventing bulk flow of the vitreous fluid [47]. Myopia and a longer axis contribute to vitreous liquefaction. It has been hypothesized that increased circulation of the vitreous fluid readily distributes oxygen from the retinal surface throughout the eye, changing the intraocular oxygen gradients and thus promoting nuclear cataract [48,49].

We expect that the current data will provide fresh ideas for investigating the pathogenesis of axial-related nuclear cataract. However, the biomarkers require multiple validation studies and clinical testing. Interactions among all the differentially expressed proteins should be studied. As an initial step, our findings provide a preliminary list of candidate biomarkers for further validation.

ACKNOWLEDGMENTS

This research was funded by the Natural Science Foundation of China (NO: 81370997) and support from the Department of Ophthalmology and Visual Sciences (DOVS) at the Washington University for Research to Prevent Blindness. We thank the Institute of Biomedical Sciences (IBS) of Shanghai

Medical School, Fudan University, for its assistance in iTRAQ reagent labeling, 2D-LC and MS/MS. We also gratefully acknowledge the patients and research participants who contributed samples for this study. The authors have declared no conflict of interest.

REFERENCES

1. Resnikoff S, Keys TU. Future trends in global blindness. Indian J Ophthalmol 2012; 60:387-95. [PMID: 22944747].
2. Ono K, Hiratsuka Y, Murakami A. Global inequality in eye health: country-level analysis from the Global Burden of Disease Study. Am J Public Health 2010; 100:1784-8. [PMID: 20634443].
3. Brian G, Taylor H. Cataract blindness-challenges for the 21st century. Bull World Health Organ 2001; 79:249-56. [PMID: 11285671].
4. Grosvenor T. Why is there an epidemic of myopia? Clin Exp Optom 2003; 86:273-5. [PMID: 14558848].
5. Saw SM, Gazzard G, Shih-Yen EC, Chua WH. Myopia and associated pathological complica tions. Ophthalmic Physiol Opt 2005; 25:381-91. [PMID: 16101943].
6. O'Donnell FE Jr, Maumenee AE. "Unexplained" visual loss in axial myopia: cases caused by mild nuclear sclerotic cataract. Ophthalmic Surg 1980; 11:99-01. [PMID: 7366950].
7. Wong TY, Klein BE, Klein R, Tomany SC, Lee KE. Refractive errors and incident cataracts: the Beaver Dam Eye Study. Invest Ophthalmol Vis Sci 2001; 42:1449-54. [PMID: 11381046].
8. Hoffer KJ. Axial dimension of the human cataractous lens. Arch Ophthalmol 1993; 111:914-8. [PMID: 8328932].
9. Tuft SJ, Bunce C. Axial length and age at cataract surgery. J Cataract Refract Surg 2004; 30:1045-8. [PMID: 15130642].
10. Kubo E, Kumamoto Y, Tsuzuki S, Akagi Y. Axial length, myopia, and the severity of lens opacity at the time of cataract surgery. Arch Ophthalmol 2006; 124:1586-90. [PMID: 17102006].
11. Chang MA, Congdon NG, Bykhovskaya I, Munoz B, West SK. The association between myopia and various subtypes of lens opacity: SEE (Salisbury Eye Evaluation) project. Ophthalmology 2005; 112:1395-01. [PMID: 15953641].
12. Anderson B Jr, Farmer JC Jr. Hyperoxic myopia. Trans Am Ophthalmol Soc 1978; 76:116-24. [PMID: 754368].
13. Palmquist BM, Philipson B, Barr PO. Nuclear cataract and myopia during hyperbaric oxygen therapy. Br J Ophthalmol 1984; 68:113-7. [PMID: 6691953].
14. Gesell LB, Trott A. De novo cataract development following a standard course of hyperbaric oxygen therapy. Undersea Hyperb Med 2007; 34:389-92. [PMID: 18251434].
15. Holekamp NM, Shui YB, Beebe DC. Vitrectomy surgery increases oxygen exposure to the lens: a possible mechanism for nuclear cataract formation. Am J Ophthalmol 2005; 139:302-10. [PMID: 15733992].
16. Quiram PA, Leverenz VR, Baker RM, Dang L, Giblin FJ, Trese MT. Microplasmin-induced posterior vitreous detachment affects vitreous oxygen levels. Retina 2007; 27:1090-6. .
17. Ksebs I, Brannath W, Glittenberg C, Zeiler F, Sebag J, Binder S. Posterior vitreomaeular adhesion: a potential risk factor for exudative age-related macular degeneration. Am J Ophthalmol 2007; 144:741-6. .
18. Murakami T, Takagi H, Ohashi H, Kita M, Nishiwaki H, Miyamoto K, Watanabe D, Sakamoto A, Yamaike N, Yoshimura N. Role of posterior vitreous detachment induced by intravitreal tis sue plasminogen activator in macular edema with central retinal vein occlusion. Retina 2007; 27:1031-7. [PMID: 18040240].
19. Boscia F, Grattagliano I, Vendemiale G, Micelli-Ferrari T, Altomare E. Protein oxidation and lens opacity in humans. Invest Ophthalmol Vis Sci 2000; 41:2461-5. [PMID: 10937554].
20. Micelli-Ferrari T, Vendemiale G, Grattagliano I, Boscia F, Arnese L, Altomare E, Cardia L. Role of lipid peroxidation in the pathogenesis of myopic and senile cataract. Br J Ophthalmol 1996; 80:840-3. [PMID: 8942384].
21. Lapko VN, Cerny RL, Smith DL, Smith JB. Modifications of human betaA1/betaA3- crystal lins include S-methylation, glutathiolation, and truncation. Protein Sci 2005; 14:45-54. [PMID: 15576560].
22. Hains PG, Truscott RJ. Post-translational modifications in the nuclear region of young, aged, and cataract human lenses. J Proteome Res 2007; 6:3935-43. [PMID: 17824632].
23. Miao A, Zhang X, Jiang Y, Chen Y, Fang Y, Ye H, Chu R, Lu Y. Proteomic analysis of SRA01/04 transfected with wild-type and mutant HSF4b identified from a Chinese congenital cataract family. Mol Vis 2012; 18:694-704. [PMID: 22509099].
24. Truscott RJ, Comte-Walters S, Ablonczy Z, Schwacke JH, Berry Y, Korlimbinis A, Friedrich MG, Schey KL. Tight binding of proteins to membranes from older human cells. Age (Dordr) 2011; 33:543-54. [PMID: 21181282].
25. Hoehenwarter W, Klose J, Jungblut PR. Eye lens proteomics. Amino Acids 2006; 30:369-89. [PMID: 16583312].
26. Wu WW, Wang G, Baek SJ, Shen RF. Comparative study of three proteomic quantitative methods, DIGE, cICAT, and iTRAQ, using 2D gel-or LC-MALDI TOF/TOF. J Proteome Res 2006; 5:651-8. [PMID: 16512681].
27. Zhou HY, Yan H, Wang LL, Yan WJ, Shui YB, Beebe DC. Quantitative proteomics analysis by iTRAQ in human nuclear cataracts of different ages and normal lens nuclei. Proteomics Clin Appl 2015; 9:776-86. [PMID: 25418515].
28. Chylack LT Jr, Leske MC, McCarthy D, Khu P, Kashiwagi T, Sperduto R. Lens opacities classification system II (LOCS II). Arch Ophthalmol 1989; 107:991-7. [PMID: 2751471].
29. Harrington V, Srivastava OP, Kirk M. Proteomic analysis of water insoluble proteins from normal and cataractous human lenses. Mol Vis 2007; 13:1680-94. [PMID: 17893670].

30. Srivastava OP. Age-related increase in concentration and aggregation of degraded polypep tides in human lenses. Exp Eye Res 1988; 47:525-43. [PMID: 3181333].

31. Hains PG, Truscott RJ. Post-translational modifications in the nuclear region of young, aged, and cataract human lenses. J Proteome Res 2007; 6:3935-43. [PMID: 17824632].

32. Miao A, Zhang X, Jiang Y, Chen Y, Fang Y, Ye H, Chu R, Lu Y. Proteomic analysis of SRA01/04 transfected with wild-type and mutant HSF4b identified from a Chinese congenital cataract family. Mol Vis 2012; 18:694-704. [PMID: 22509099].

33. Zhang X, Yin X, Yu H, Liu X, Yang F, Yao J, Jin H, Yang P. Quantitative proteomic analysis of serum proteins in patients with Parkinson's disease using an isobaric tag for relative and absolute quantification labeling, two-dimensional liquid chromatography, and tandem mass spectrometry. Analyst (Lond) 2012; 137:490-5. [PMID: 22108571].

34. Chen G, Zhang Y, Jin X, Zhang L, Zhou Y, Niu J, Chen J, Gu Y. Urinary proteomics analysis for renal injury in hypertensive disorders of pregnancy with iTRAQ labeling and LC-MS/MS. Proteomics Clin Appl 2011; 5:300-10. [PMID: 21538910].

35. Xia CH, Cheung D, DeRosa AM, Chang B, Lo WK, White TW, Gong X. Knock-in of alpha3 connexin prevents severe cataracts caused by an alpha8 point mutation. J Cell Sci 2006; 15:2138-44. [PMID: 16687738].

36. Molina SA, Takemoto DJ. The role of Connexin 46 promoter in lens and other hypoxic tis sues. Commun Integr Biol 2012; 5:114-7. [PMID: 22808311].

37. Hansen L, Yao W, Eiberg H, Funding M, Riise R, Kjaer KW, Hejtmancik JF, Rosenberg T. The congenital "ant-egg" cataract phenotype is caused by a missense mutation in connex in46. Mol Vis 2006; 12:1033-9. [PMID: 16971895].

38. Guleria K, Sperling K, Singh D, Varon R, Singh JR, Vanita V. A novel mutation in the connexin 46 (GJA3) gene associated witdomi nant congenital cataract in an Indian family. Mol Vis 2007; 13:1657-65. [PMID: 17893674].

39. Yoshida M, Harada Y, Kaidzu S, Ohira A, Masuda J, Nabika T. New genetic model rat for congenital cataracts due to a connexin 46 (Gja3) mutation. Pathol Int 2005; 55:732-7. [PMID: 16271086].

40. Chang B, Wang X, Hawes NL, Ojakian R, Davisson MT, Lo WK, Gong XA. Gja8 (Cx50) point mutation causes an alteration of alpha 3 connexin (Cx46) in semi-dominant cataracts of Lop10 mice. Hum Mol Genet 2002; 11:507-13. [PMID: 11875045].

41. Graw J, Löster J, Soewarto D, Fuchs H, Meyer B, Reis A, Wolf E, Balling R, Hrabé de Angelis M. Characterization of a mutation in the lens-specific MP70 encoding gene of the mouse leading to a dominant cataract. Exp Eye Res 2001; 73:867-76. [PMID: 11846517].

42. Zhang J, Li J, Huang C, Xue L, Peng Y, Fu Q, Gao L, Zhang J, Li W. Targeted knockout of the mouse betaB2-crystallin gene (Crybb2) induces age-related cataract. Invest Ophthalmol Vis Sci 2008; 49:5476-83. [PMID: 18719080].

43. Ueda Y, Duncan MK, David LL. Lens proteomics: the accumulation of crystallin modifica tions in the mouse lens with age. Invest Ophthalmol Vis Sci 2002; 43:205-15. [PMID: 11773033].

44. Lampi KJ, Ma Z, Hanson SR, Azuma M, Shih M, Shearer TR, Smith DL, Smith JB, David LL. Age-related changes in human lens crystallins identified by two-dimensional electropho resis and mass spectrometry. Exp Eye Res 1998; 67:31-43. [PMID: 9702176].

45. Feng J, Smith DL, Smith JB. Human lens β-crystallin stability. J Biol Chem 2000; 275:11585-90. [PMID: 10766773].

46. Zhang Z, David LL, Smith DL, Smith JB. Resistance of human betaB2-crystallin to in vivo modification. Exp Eye Res 2001; 73:203-11. [PMID: 11446770].

47. Beebe DC, Holekamp NM, Siegfried C, Shui YB. Vitreoretinal influences on lens function and cataract. Philos Trans R Soc Lond B Biol Sci 2011; 366:1293-300. .

48. Holekamp NM, Harocopos GJ, Shui YB, Beebe DC. Myopia and axial length contribute to vitreous liquefaction and nuclear cataract. Arch Ophthalmol 2008; 126:744-[PMID: 18474803].

49. Ling CA, Weiter JJ, Buzney SM, Lashkari K. Competing theories of cataractogenesis after pars plana vitrectomy and the nutrient theory of cataractogenesis: a function of altered aqueous fluid dynamics. Int Ophthalmol Clin 2005; 45:173-98. [PMID: 16199976].

Articles are provided courtesy of Emory University and the Zhongshan Ophthalmic Center, Sun Yat-sen University, P.R. China. The print version of this article was created on 31 July 2016. This reflects all typographical corrections and errata to the article through that date. Details of any changes may be found in the online version of the article.